Granular Matter (2016) 18:34
DOI 10.1007/s10035-016-0637-x

ORIGINAL PAPER

Ordering and stress transmission in packings of straight and curved spherocylinders

G. Lu[1] · R. C. Hidalgo[2] · J. R. Third[1] · C. R. Müller[1]

Received: 24 June 2015

Abstract In this work we apply the discrete element method (DEM) to model packings of spherocylinders. The so-called composite spheres method was used to construct particles of different aspect ratio, surface shape and curvature. Using the DEM we probe in detail the effect of particle curvature and surface shape on packing morphology and stress transmission. We find that particle shape has a remarkable influence on both the packing morphology (quantified via the solid fraction, particle orientation distribution and radial distribution function) and stress transmission. Specifically, elongated particles have a high preference for horizontal alignment, whereas an increasing particle curvature leads to a more continuous (i.e. less discrete) particle orientation distribution. Generally, we observe that rough and curved particles have a stronger tendency for interlocking (in particular for small particle aspect ratios, i.e. $AR = 2$ and 3) leading to the formation of dense packing structures. In addition packings of rough and curved particles of small aspect ratios favor stress transmission in the gravitational direction, thus, limiting stress saturation with depth.

Keywords Particle packing · Non-spherical particles · Particle ordering · Stress transmission · Discrete element method (DEM)

✉ C. R. Müller
muelchri@ethz.ch

R. C. Hidalgo
raulcruz@unav.es

[1] Department of Mechanical and Process Engineering, Institute of Energy Technology, ETH Zürich, Leonhardstrasse 21, 8092 Zürich, Switzerland

[2] Departamento de Física, Facultad de Ciencias, Universidad de Navarra, 31080 Pamplona, Spain

List of symbols

A	Particle cross-sectional area (m^2)
AR	Particle aspect ratio (−)
d_p	Primary sphere diameter (m)
dt	Time step of DEM simulations (s)
E_k	Kinetic energy (J)
E_p	Elastic potential energy (J)
f_{ij}	Contact force between particles i and j (N)
F_n	Normal force (N)
F_t	Tangential force (N)
$G\,(r)$	Radial distribution function (−)
h	Dimensionless packing depth (−)
h_c	Characteristic depth of packing (−)
H	Height of container (m)
k_n	Normal spring stiffness (N/m)
k_t	Tangential spring stiffness (N/m)
l_{axial}	Length of particle major axis (m)
m	Particle mass (kg)
N	Number of particles (−)
P_0	Stress (N/m)
P_j	Saturation stress (N/m)
r, $\mathbf{r}$	Distance/vector relative to a point (m)
δr	Differential distance (m)
v_n	Relative normal velocity (m/s)
v_t	Relative tangential velocity (m/s)
W	Width of container (m)
X, Y	Coordinates (m)

Greek letters

δ_n	Particle overlap (m)
δ_t	Tangential displacement (m)
η_n	Normal damping factor (−)

Published online: 05 May 2016

η_t	Tangential damping factor (−)
γ	Particle orientation angle (°)
μ	Coefficient of friction (−)
ϕ	Solid fraction (−)
ρ	Number of particles per unit area (1/m^2)
ρ_p	Particle density (kg/m^3)
θ	Angle of curvature (°)
ω	Coarse-graining scale (−)
σ_v	Major eigenvalue of stress tensor (N/m)
σ_h	Minor eigenvalue of stress tensor (N/m)
$\bar{\sigma}_{\alpha\beta}$ (**r**)	Mean stress tensor (N/m)
φ (**r**)	Gaussian coarse-graining function (1/m^2)

1 Introduction

Granular packings are frequently encountered in nature and industry [1]. However, experimental studies on granular packings are inherently difficult due to their opacity, thus, making the use of optical measurement techniques largely impossible [2]. On the other hand, the advancement of computational techniques, in particular the so-called discrete element method (DEM) [3] has opened new routes to probe the physics of granular packings [4,5]. DEM allows us to perform numerical 'measurements' in granular system, providing e.g. information about the contact forces acting between particles. Importantly, DEM is capable of modelling particles of non-spherical shape [6–8]; a crucial aspect, considering that the morphology and the mechanical properties of packings are strongly affected by particle shape [9,10].

So far, the majority of both experimental and numerical studies have considered packings of spherical particles only [5]. However, the appropriate description of packings composed of non-spherical particles is of significant importance for practical applications such as the handling of rocks, rice, wheat or tablets [11]. Hence, in recent years packings of highly anisotropic particles have received increasing attention [12–26]. These studies have revealed that most structural properties displayed by packings of isotropic granular media cannot be extrapolated easily to (highly) anisotropic particle system.

For example, it is well known that elongated particles can pack more densely when compared to spheres [10]. However, the packing density reaches also a maximum at a certain aspect ratio [15]. A similar trend was observed for the coordination number, viz. the mean number of contact points of a particle. In addition, in packings of elongated particles a preferred particle alignment along their major axis was shown experimentally [21] and numerically [15,22]. These ordered structures are believed to affect notably the transmission of stress in the packing. For example, Azéma and Radjaï [24,25] performed two-dimensional, bi-axial compression tests on packings composed of cylinder-shaped particles. They observed a linear increase of the shear strength of the material with increasing particle elongation. This phenomenon was attributed to the ordering of particles on a mesoscopic scale. Similarly, Hidalgo et al. [21,22] found a preferred particle alignment in the horizontal direction for quasi-2D packings of steel rods. In such packings, the authors could not observe a saturating stress with increasing packing height. Instead, a stress profile similar to the linear hydrostatic stress profile was recorded. However, the ordered structures disappeared when cohesive forces were introduced and the conventional stress profile (i.e. saturation with packing height) was recovered [23].

Despite recent advances in our understanding of packings composed of anisotropic particles, several questions concerning their mechanical properties are still open. For example, it is still unclear how the surface shape of the particles influences a packing's morphology and stress transmission. A better understanding of this effect is important as most granular media possess uneven surfaces, e.g. gravel, rocks or agricultural goods. In addition, the effect of particle curvature on the packing properties is also not well understood. This is particularly important for the handling of fibrous materials, e.g. cellulose fibers. Thus, this work addresses the question how particle surface shape and curvature affect a packing's structure and stress transmission.

2 Numerical system setup

In this work, we examined two-dimensional granular packings using the DEM. The composite spheres method was used to simulate non-spherical particles [10]. A linear spring and dash-pot model was implemented to model the contact forces. For two colliding particles (i and j) the contact force acting in the normal direction was given by

$$F_n = \max\left(0, k_{n_{ij}}\delta_n - 2\eta_n\sqrt{m_{ij}k_{n_{ij}}}v_n\right) \tag{1}$$

Here δ_n is the overlap between the contacting spheres, η_n is the normal damping factor, v_n is the relative velocity in the normal direction and m_{ij} is the effective mass given by $1/m_{ij} = 1/m_i + 1/m_j$. The effective normal stiffness was calculated as $1/k_{n_{ij}} = 1/k_{n_i} + 1/k_{n_j}$. In the tangential direction, the maximal contact force was limited by Coulomb's law of friction, viz.

$$F_t = \min\left(\mu k_{n_{ij}}\delta_n, k_{t_{ij}}\delta_t - 2\eta_t\sqrt{m_{ij}k_{t_{ij}}}v_t\right), \tag{2}$$

where μ, η_t and v_t are the coefficient of friction, the tangential damping factor and the relative velocity in the tangential direction, respectively. The tangential displacement, δ_t, was given by $\delta_t = \int v_t dt$ and the effective tangential stiffness was determined as $1/k_{t_{ij}} = 1/k_{t_i} + 1/k_{t_j}$. The time step dt

Table 1 Mechanical parameters of the particles modelled

Parameter	Symbol	Value
Particle density	ρ	2500 kg/m^3
Normal spring stiffness	k_n	2000 N/m
Tangential spring stiffness	k_t	1000 N/m
Normal damping factor	η_n	0.2
Tangential damping factor	η_t	0.2
Coefficient of friction	μ	0.3
Primary sphere diameter	d_p	3×10^{-3} m

employed in the DEM simulations was set to 1.1×10^{-5} s, which is less than one thirtieth of the duration of a binary collision between particles. A third order Adams–Bashforth integration scheme was implemented to update the particle velocities and positions. Table 1 shows the mechanical parameters of the particles modelled in this work. We have performed additional simulations to assess the sensitivity of our conclusions drawn to the mechanical parameters of the particles. We found that varying k_n in the range 1000–4000 N/m (correspondingly k_t in the range 500–2000 N/m), η_n and η_t in the range 0.1–0.4, and μ in the range 0.1–0.5 did not affect the conclusions drawn in this work.

Elongated spherocylinders composed of several primary spheres were considered. The aspect ratio of a straight spherocylinder was defined as the ratio between its axial length and the diameter of a primary sphere, i.e. $AR = l_{axial}/d_p$ as shown in Fig. 1a. A uniform size distribution of ±5 % was applied to the primary spheres (average diameter 3 mm) used to model non-spherical particles. The simulations were purely two-dimensional, i.e. the particles cannot move in the z direction and cannot rotate about any axis in the xy plane (Fig. 1). The height of the container was $h = 2.0$ m. In order to compare the numerical results of the systems containing particles of different aspect ratios, the width of the container, W, was set to 20 times the major axis of the particle l_{axial}, i.e. $W = 20 l_{axial}$. The walls of the container had the same normal and tangential stiffness as the particles. In total 9000 particles were simulated.

Packings were generated by initializing first horizontal lines of particles, located 1.985 m above the bottom of the container. Each particle was initialized with a random orientation angle and a random horizontal velocity (in the range −0.025 to +0.025 m/s). A new line of particles was generated, once the previous line of particles had settled 0.021 m under gravity. The filling rate was approximately 270 particles per second. Once all particles had settled, the system was allowed to relax until its mean kinetic energy E_k was at least five orders of magnitude lower than its elastic potential energy $E_p = \sum \frac{1}{2} k \delta^2$). Subsequently, the morphology of the consolidated packing was analyzed. For each configuration, 30 repetitions were performed using different initial conditions, i.e. different initial velocities and particle orientations.

In the first set of numerical experiments the effect of the particle aspect ratio ($AR = 2$, 3, 5, and 7) and surface shape on the packing morphology and stress transmission through the bed was studied. Here, the packing of spheres served as a reference case. The surface shape of the spherocylinders was manipulated by varying the overlap of the primary spheres (zero overlap or 50 % overlap) as shown in Fig. 1a, b. Since our aim was to study the effect of surface shape on the packing characteristics, it was ensured that the mass and the inertia tensor of the smooth and coarse particles were identical. During the initialization step the mass of the coarse particles was set to the mass of the smooth particles with the same aspect ratio. In addition the inertia tensor of the coarse particles was calculated in a body (particle)-fixed (or local) coordinate system, chosen such that the inertia tensor contained non-zero values only along its diagonal. The values of the inertia tensor of the smooth particles (in the body-fixed coordinate system) were set to the same values as the inertia tensor of the coarse particles of identical aspect ratio. A side effect of this approach was that the density of the primary spheres varied, resulting in a non-uniform density distribution in smooth particles.

In the second set of numerical experiments, the effect of particle curvature on the packing morphology and stress transmission was assessed. Here, smooth spherocylinders of aspect ratios $AR = 3$, 5, and 7 were used (in the packings simulated the aspect ratios had a distribution in the range 95.2–105.3 %). The curved particles were modelled as proposed by Nan et al. [19]. A curved spherocylinder, Fig. 1c, was characterized by two parameters viz. its aspect ratio and angle of curvature. The aspect ratio was the ratio between the axial length of the particle to the diameter of a primary sphere. The angle of curvature, θ, was defined as the ratio of the length of the particle torus (measured along the curved axis of the particle) and the curvature radius (Fig. 1c). As limiting cases, $\theta = 0°$ corresponds to a straight particle, while $\theta = 180°$ represents a semicircle. The angle of curvature was varied from 30° to 120° using a step size of 30°. The mass of a curved spherocylinder was equal to the mass of the corresponding straight spherocylinder of identical aspect ratio. However, due to the particle curvature, the inertia tensor of a curved spherocylinder was different to that of a straight spherocylinder of the same aspect ratio.

3 Results and discussion

3.1 Effect of surface shape on packing morphology and stress transmission

Figure 1 shows packings of straight spherocylinders (aspect ratio $AR = 5$) of different surface shape. For comparison, the packing of curved spherocylinders (aspect ratio $AR = 5$,

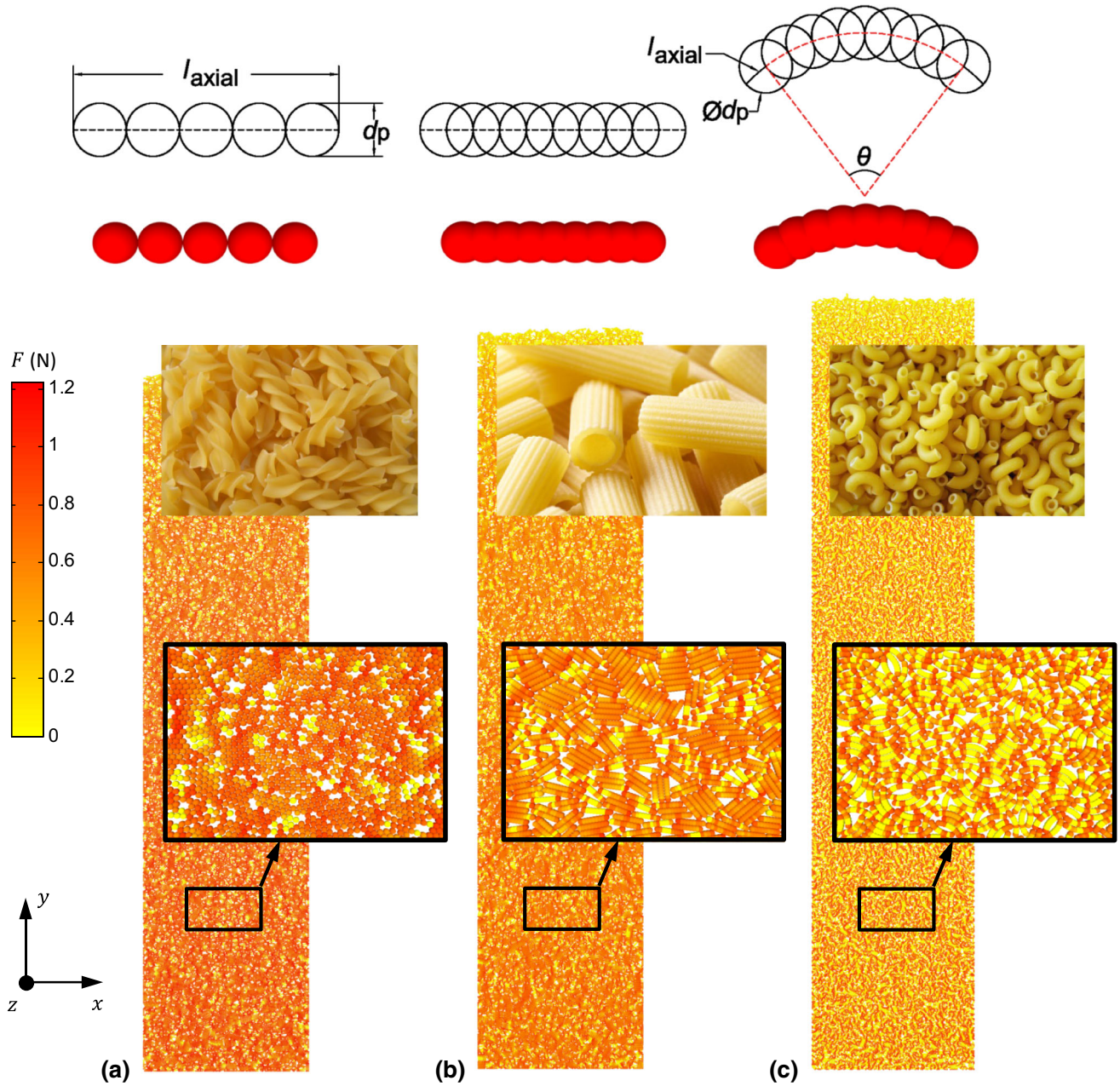

Fig. 1 Packings of **a** straight, coarse spherocylinders of $AR = 5$, **b** straight, smooth spherocylinders of $AR = 5$, and **c** curved spherocylinders (angle of curvature: $\theta = 60°$) of $AR = 5$. The *colour* indicates the magnitude of the contact forces acting on the primary spheres [(including contact forces between particles and walls (the bottom and the lateral walls)]. The shapes of the particles simulated can be related to for example different types of pasta [27–29]

angle of curvature $\theta = 60°$) is also illustrated. The colour of the particles indicates the magnitude of the contact forces acting on the individual particles. Note that due to a larger number of primary spheres, the volume of a straight, smooth particle is larger compared to its coarse counterpart (see Table 2, particle cross-sectional area A). From Fig. 1 it is also noticeable that coarse particles form highly ordered structures. In addition, curved spherocylinders lead to higher and looser deposits when compared to the corresponding straight particle systems. This observation can be attributed to a more pronounced 'excluded volume' effect for curved particles. The 'excluded volume' in a deposit refers to the void region around a particle that cannot be occupied by other particles of the same size and shape [16].

The packings obtained were first characterized by calculating the spatially resolved solid fraction. Here, we have

Table 2 Mean solid fraction ϕ obtained in packings of particles with different aspect ratios and surface shapes

Aspect ratio AR	Coarse particle A	Coarse particle ϕ	Smooth particle A	Smooth particle ϕ
2	1.41×10^{-5} m^2	0.87 ± 0.0021	1.57×10^{-5} m^2	0.88 ± 0.0007
3	2.12×10^{-5} m^2	0.81 ± 0.0009	2.43×10^{-5} m^2	0.87 ± 0.0009
5	3.53×10^{-5} m^2	0.76 ± 0.0013	4.15×10^{-5} m^2	0.85 ± 0.0015
7	4.95×10^{-5} m^2	0.73 ± 0.0015	5.87×10^{-5} m^2	0.82 ± 0.0020

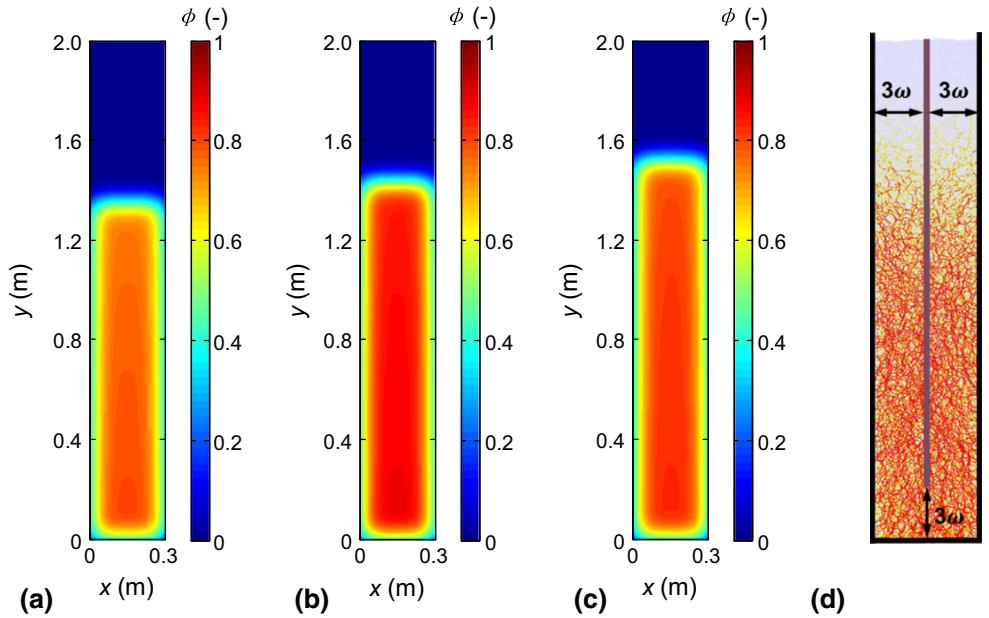

Fig. 2 Spatially resolved solid fractions of different packings: **a** straight, coarse spherocylinders with $AR = 5$, **b** straight, smooth spherocylinders with $AR = 5$, and **c** curved spherocylinders (angle of curvature $\theta = 60°$) with $AR = 5$; **d** schematic showing the *central vertical slice* that was used for further analysis of the packing structure

implemented a coarse-grain averaging technique to examine the solid fraction (as well as the stress fields) of the packing. The coarse-grained solid fraction was obtained as $\phi(\mathbf{r}) = \sum_{i=1}^{N} A_i \varphi(\mathbf{r} - \mathbf{r}_i)$, where A_i is the cross-sectional area of a particle. In this context, a Gaussian coarse-graining (CG) function $\varphi(\mathbf{r}) = \frac{1}{2\pi\omega^2} e^{-\left(\mathbf{r}/\sqrt{2}\omega\right)^2}$, with a coarse-graining scale ω was applied [30]. In all cases, ω was set to $3 \times AR \times d_p$ (d_p is the diameter of the primary spheres), which was consistent with the value chosen by Acevedo et al. [31] for rod-shaped particles. The spatially resolved solid fractions $\phi(\mathbf{r})$ obtained are plotted in Fig. 2. Note that the value of ω is sufficiently small to capture accurately the spatial variation of the solid. In all packings assessed, the color maps show a rather uniform solid fraction in the centre of the bed (only a slight increase towards the bottom of the container is observed). Figure 2 also shows that coarse spherocylinders ($AR = 5$) pack less densely than straight, smooth spherocylinders of the same aspect ratio. Furthermore, packings of curved, smooth spherocylinders show a lower solid fraction than their straight counterparts. The further analysis of the structure of the different packings is now restricted to the central vertical section ($\Delta = 2 \times AR \times d_p$ wide) of the bed (see Fig. 2d), which is located 3ω away from the lateral and bottom walls [32]. The mean solid fractions obtained in this region are summarized in Table 2. Here we observe that the solid fraction decreases with increasing aspect ratio, independent of the surface shape. This observation is consistent with experimental findings in packings of two-dimensional rods [22] and is attributed to an increasing resistance to particle re-arrangement for increasing particle aspect ratios [33].

The morphology of the packings was characterized in more detail by determining the particle orientation distributions (Fig. 3). The particle orientation angle γ was defined as the angle formed by the principal axis of the particle and the horizontal axis of the system. Figure 3 plots the distribution of the orientation of spherocylinders of different aspect ratios and surface shapes. To exclude wall effects, only the central section of the packing was used for data analysis, i.e. particles located within the distance $AR \times d_p$

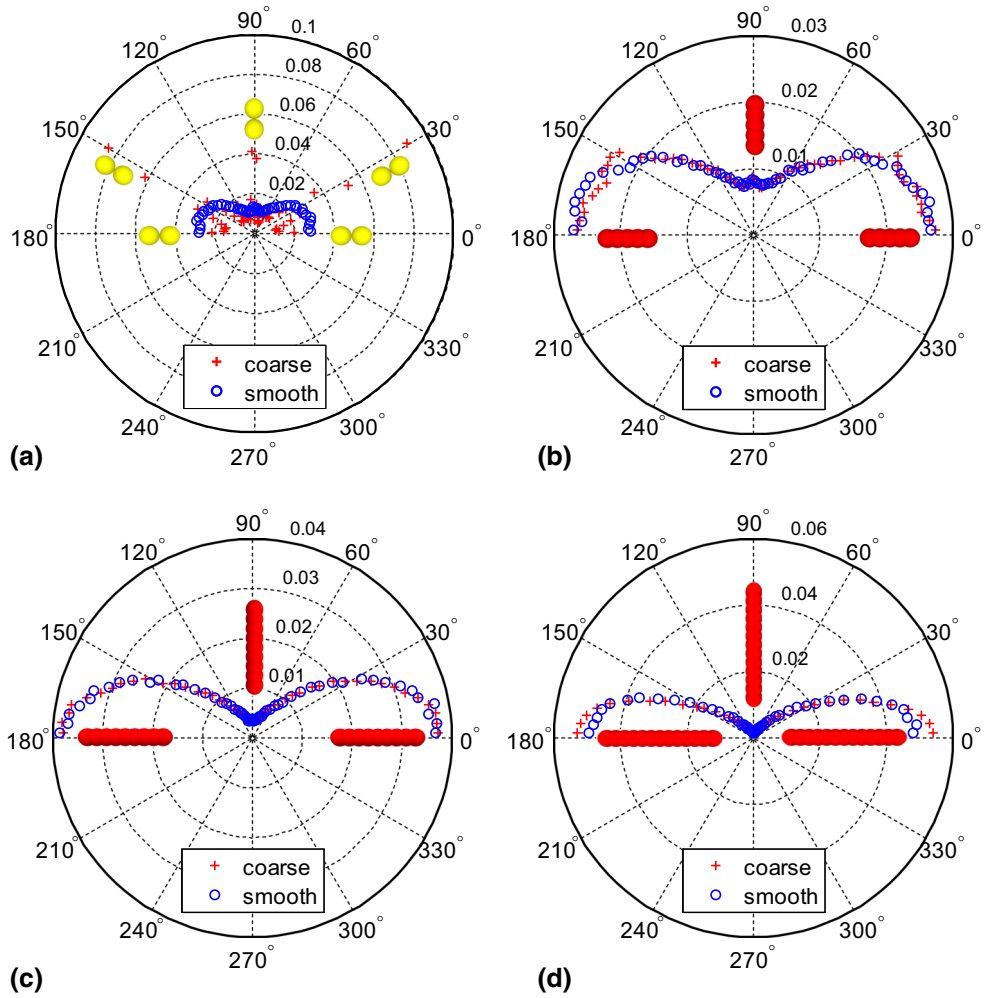

Fig. 3 Distribution of particle orientation for spherocylinders with **a** $AR = 2$, **b** $AR = 3$, **c** $AR = 5$, and **d** $AR = 7$ ('+': coarse particles; '◯': smooth particles)

from the walls were disregarded. Figure 3 shows clearly that an increase in particle aspect ratio enhances the tendency of particles to align horizontally ($\gamma = 0°$ and 180°). This observation is in agreement with experimental measurements obtained in packings of elongated, faceted particles [21,22]. However, in our simulations we could also observe that the particle surface shape has a notably influence on the particle orientation distribution. For instance, coarse particles with $AR = 2$ (dimers) orientated largely at specific angles, viz. $\gamma = 0°$, 30°, 90°, 150°, and 180°. These characteristic orientations indicate the existence of locally ordered structures. Interestingly, we could not observe any peak in the particle orientation distribution at 60° and 120°, implying that these more vertically-oriented positions are not stable for the dimers. On the other hand, smooth particles with $AR = 2$ did not show such highly anisotropic behaviour, i.e. an appreciably less discrete particle orientation distribution was observed. Similarly, for $AR = 3$, the surface shape affected notably the particle orientation distribution. Coarse particles show local maxima in their orientation distribution at $\gamma = 30°$ and 150°, whereas smooth particles align with the horizontal axis with the highest probability. For $AR > 3$, the differences in the orientation distribution between coarse and smooth particles largely disappear. Nonetheless, for $AR = 7$, coarse particles still align slightly more favorably with the horizontal axis ($\gamma = 0°$ and 180°). This effect was not observed for $AR = 5$.

The packings were characterized further by calculating their radial distribution function (RDF), given as $G(r) = N(r + \delta r)/2\pi r \delta r \rho$. Here, ρ is the number of particles per unit area averaged over the analysis region and $N(r + \delta r)$ accounts for the number of particles with their mass centers located in the differential area $2\pi r \delta r$ relative to a measuring point. For a random packing of monodisperse spheres $G(r)$ equals to 1. In this analysis, only particles that are located in the central area of the packing were considered, i.e. only particles with a distance larger than $(10 + AR) \times d_p$ from the walls were analyzed. In this work an incremental

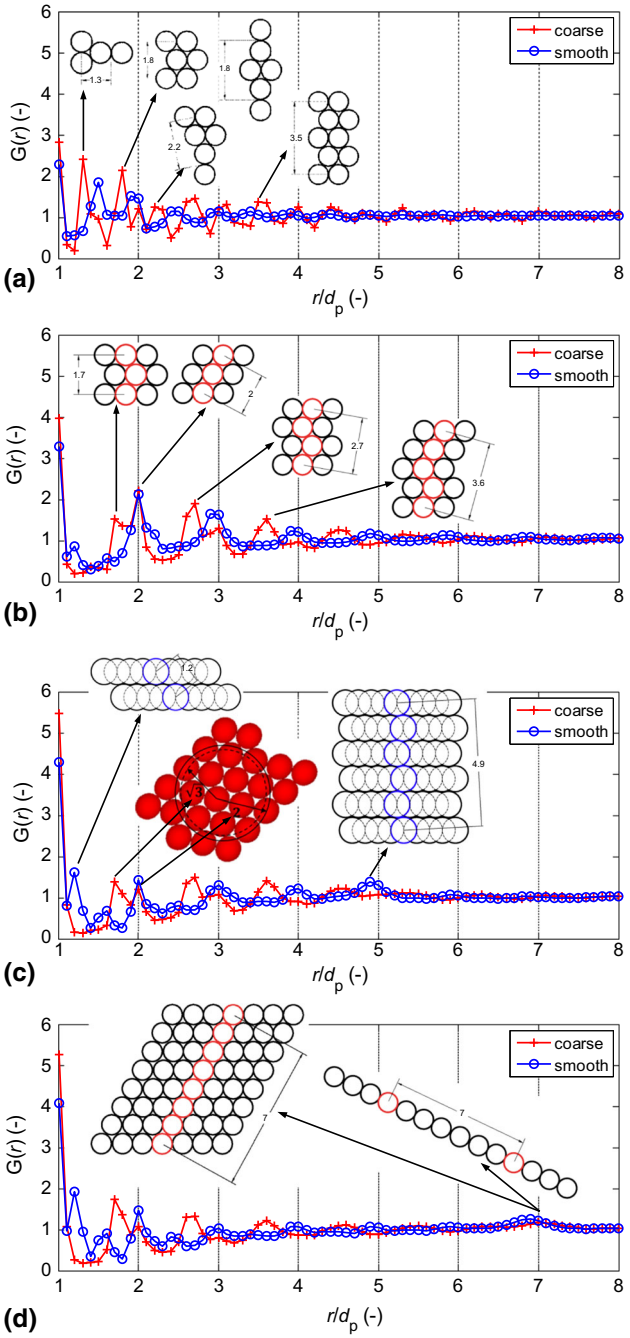

Fig. 4 Radial distribution function (RDF) of packings of spherocylinders: **a** $AR = 2$, **b** $AR = 3$, **c** $AR = 5$, and **d** $AR = 7$ ('+': coarse particle; '◯': smooth particle). Packing configurations that correspond to specific peaks in the RDFs are illustrated. To aid the reader, the central primary sphere of each spherocylinder is marked in *red* (coarse spherocylinder) or *blue* (smooth spherocylinder) (colour figure online)

radius of $\delta r = 0.3$ mm was used. In Fig. 4, the RDFs of the different packings studied are plotted. Several packing configurations that correspond to distinct peaks in the RDFs are drawn to aid the reader. A general observation that can be made from the data plotted in Fig. 4 is that $G(r)$ approaches asymptotically $G(r) = 1$. A further observation from Fig. 4 is that coarse particles possess more pronounced peaks in their RDF, indicative of a higher tendency to form crystalized structures. This effect can be explained by the facile interlocking of multiple coarse particles. For example, for coarse particles with $AR = 2$, $G(r)$ exhibits several distinct peaks that correlate with specific packing arrangements as illustrated in Fig. 4a. In contrast, smooth particles with $AR = 2$ show fewer peaks in their RDF and the peaks observed are due to particle alignment along the principal axis only. In line with this observation is the fact that for smooth particles the RDF approaches 1 faster (when compared to coarse particle packings). A further evidence of particle interlocking is the fact that the peaks in the RDF of coarse particles are shifted to lower r values compared to smooth particles. Similar observations can be made for elongated particles, i.e. $AR > 2$. For instance, for $AR = 5$ the RDF of smooth particles exhibits peaks at $r/d_p \approx 1, 2, 3$, etc., which correspond to structures in which $2, 3, 4$, etc. particles align horizontally with each other. In packings of coarse particles the peaks are shifted to smaller values of r owing to the interlocking of the highly concave surfaces. As shown in the inset of Fig. 4c, the voids in the proximity of the concave surface of a coarse particle can be readily occupied by neighbouring particles, thus leading to a pronounced peak at e.g. $r/d_p = 1.7$ (besides the peak formed at $r/d_p = 2$). From the RDFs plotted it is clear that the surface shape of a particle influences critically local particle structures and particle alignments. Furthermore, comparing the peak heights of the RDFs of packings of coarse and smooth particles it can be concluded that crystalized structures are more pronounced in packings of coarse particles than for smooth particles.

Next we examined the micromechanical properties of the granular packings allowing us to gain additional insight into the relationship between the microstructure of a packing and stress transmission. To this end, the mean stress tensor $\bar{\sigma}_{\alpha\beta}(\mathbf{r})$ as defined by Goldhirsch [30] was calculated:

$$\bar{\sigma}_{\alpha\beta}(\mathbf{r}) = -\frac{1}{2}\sum_{i,j;i\neq j} f_{ij\alpha} r_{ij\beta} \int_0^1 ds\varphi\left(\mathbf{r} - \mathbf{r}_i + s\mathbf{r}_{ij}\right) \qquad (3)$$

In Eq. 3 the sum runs over all contacting particles i and j whose center of mass is located at $\mathbf{r}_i$ and $\mathbf{r}_j$, respectively. Here, $\mathbf{r}_{ij} \equiv \mathbf{r}_j - \mathbf{r}_i$ is the vector joining the two centers of mass of two colliding particles. The contact force exerted by particle j on particle i is given by f_{ij}, which points from particle j to particle i. $\varphi(\mathbf{r})$ is the coarse-grained function. In all cases studied $\omega = 3 \times AR \times d_p$. Additional analyses using $\omega = 2 \times AR \times d_p$ showed that the stress, σ, obtained using different coarse-graining scales ω were very similar. To avoid wall effects, the analysis was restricted to the central vertical section located 3ω away from both the bottom and

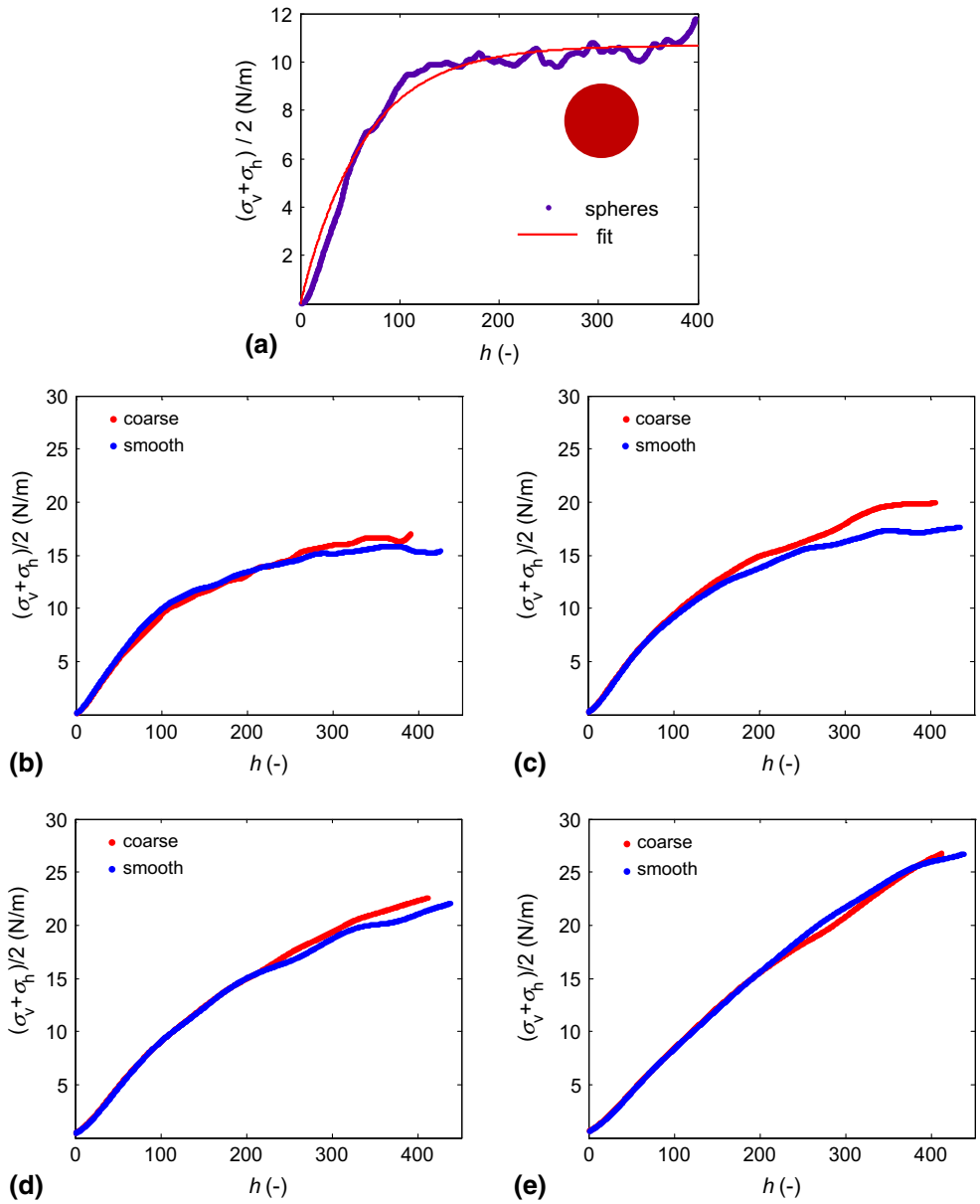

Fig. 5 Stress profile in a packing of spheres or spherocylinders: $P_0 = (\sigma_v + \sigma_h)/2$ as a function of the normalized packing depth h (normalized by d_p) for packings of **a** spheres and **b**–**e** elongated, coarse and smooth spherocylinders with **b** $AR = 2$, **c** $AR = 3$, **d** $AR = 5$, and **e** $AR = 7$. For the packing of spheres, the numerical data is fitted to $P_0 = P_j(1 - e^{-h/h_c})$

the lateral walls (see Fig. 2d). In regions close to the walls a more accurate coarse-graining description should be used [32].

For reference, in Fig. 5a the stress $P_0 = (\sigma_v + \sigma_h)/2$, obtained in a packing of spheres, is also plotted (σ_v and σ_h are, respectively, the major (vertical direction) and the minor (horizontal direction) eigenvalues of the mean stress tensor $\bar{\sigma}_{\alpha\beta}(\mathbf{r})$. The packing depth h is defined as the vertical distance ranging from the surface of the packing to a certain position in the packing. The packing depth is normalized by d_p. Here "surface" refers to the highest surface level recorded in 30 simulation repetitions. Note that the differences in the packing height were very small i.e. generally less than $5 \times d_p$. As expected a Janssen-type stress profile [34] was obtained in a packing of spheres and the numerical data can be fitted well by $P_0 = P_j\left(1 - e^{-h/h_c}\right)$, where P_j is the saturation stress and h_c is the characteristic depth of the packing. Figure 5b–e plot $P_0 = (\sigma_v + \sigma_h)/2$ as a function of the dimensionless depth h for elongated particles of different surface shape. Our simulation results show a reduced Janssen effect for elongated particles. For example, for particles with $AR = 2$, P_0 saturates with packing

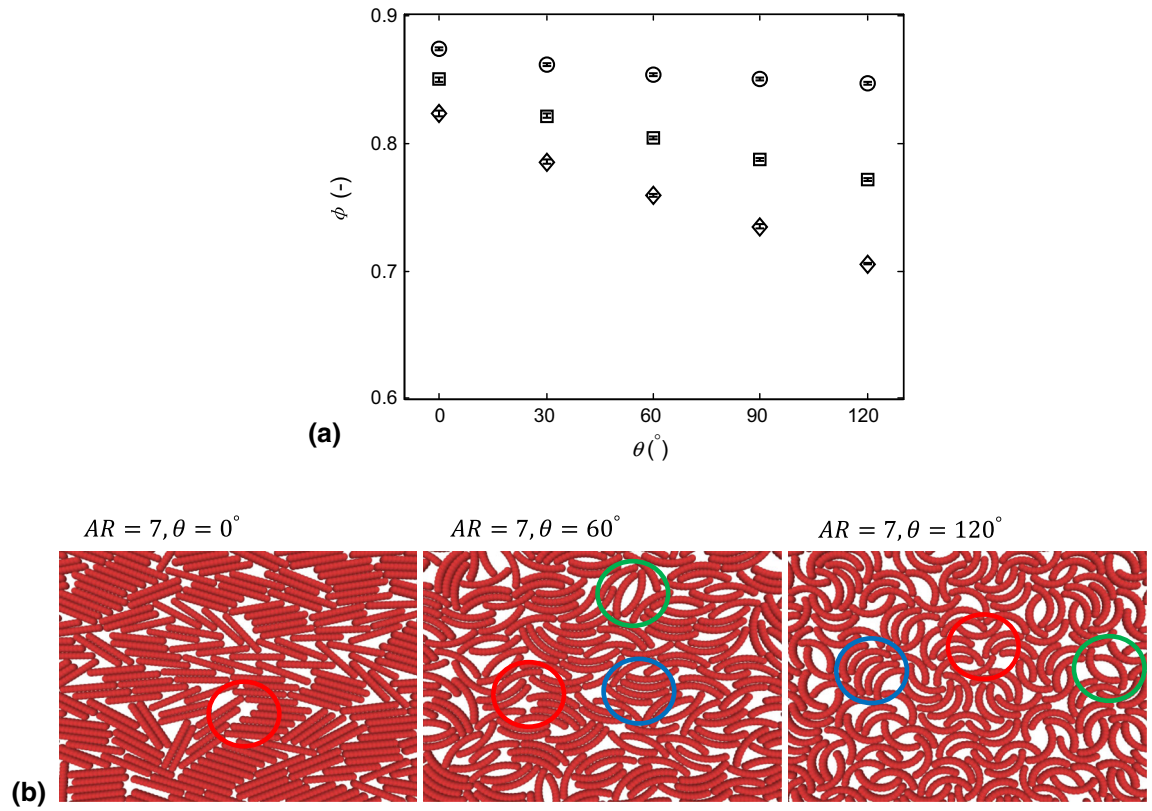

Fig. 6 Packing morphology of curved spherocylinders: **a** mean solid fraction, ϕ, as a function of curvature using spherocylinders of different aspect ratios: (◯)$AR = 3$; (□)$AR = 5$; (◇) $AR = 7$; **b** typical packing structures of cylinders with different curvatures ($AR = 7, \theta = 0°$, 60°, or 120°). For illustration, the *red circles* mark voids between local clusters, the *green circles* mark voids between two contacting particles facing each other with their concave sides and the *blue circles* mark the voids formed between convexly aligning particles (colour figure online)

depth, however, P_0 increases continuously for particles with $AR = 7$. The reduced Janssen effect is due to the preferred horizontal alignment of highly elongated particles (Fig. 3), resulting in a preferred vertical stress transmission. In addition, for a given aspect ratio an increasing surface shape leads to higher values of P_0 and a retardation in stress saturation. This effect is more pronounced for smaller aspect ratios, i.e. $AR = 2, 3$, whereas for $AR = 7$ the stress profiles do not differ appreciably for the different surface shapes modelled. These results correlate well with the structural morphologies determined for packings of coarse and smooth particles (Figs. 3 and 4). The peaks in the RDFs (Fig. 4) of coarse particles indicate interlocking during deposition, resulting in very ordered and compact local structures. This interlocking effect is particularly strong for short particles i.e. $AR = 2, 3$, which exhibit a strong preference for specific orientation angles e.g. 30° and 150° (Fig. 3). In packings of such materials P_0 converges slower to the saturation value when compared to smooth particles with the same aspect ratio. In packings of smooth particles the internal disorder induces an isotropic stress transmission resulting in a faster stress saturation. For packings of highly elongated particles i.e. $AR = 5$ and 7, particle elongation dominates the stress transmission characteristics whereas surface shape plays a minor role.

3.2 Effect of particle curvature on packing morphology and stress transmission

In the second part of this work, we examine the effect of particle curvature on packing morphology and stress transmission in packings of elongated spherocylinders. Figure 6a plots the mean solid fraction of the packings, ϕ, (in the central section of the bed, Fig. 2d) as a function of angle of curvature θ for different particle aspect ratios. For very elongated particles ($AR = 5$ and 7) the solid fraction decreases with increasing curvature. Also for particles with $AR = 3$, the solid fraction decreases with increasing curvature (up to $\theta \leq 60°$). However, for $\theta > 60°$, the solid fraction becomes nearly invariant to particle curvatures. To understand better these observations, we confirmed first that curvature does not affect significantly the cross-sectional area A of the spherocylinders. For example, increasing θ from 0° to 120° resulted in a decrease in A by only 0.77, 0.22, and 0.13 % for $AR = 3$, 5, and 7, respectively. Therefore, we can argue that the change

of solid fraction with curvature is primarily due to different packing morphologies. Figure 6b shows exemplary packings of spherocylinders ($AR = 7$) with different curvatures. Straight spherocylinders show a strong tendency for local alignment, thus reducing appreciably the void fraction of the packing. In these packings voids occur predominantly between local clusters. For an intermediate angle of curvature e.g. $\theta = 60°$, local clusters can be still observed, albeit consisting typically only of a small number of aligned particles (~ 3 particles). Large voids are formed between local clusters, or when two contacting particles face each other with their concave sides. On the other hand, small voids form between convexly aligning particles. For packings of particles with a high angle of curvature e.g. $\theta = 120°$, voids are mainly formed between particles that face each other with their concave sides or between convexly aligning particles, resulting in packings with a low solid fraction.

The structure of packings composed of curved spherocylinders was analyzed further by calculating the particle orientation distribution and the radial distribution function (RDF). Figure 7 plots the particle orientation distribution for $AR = 3$, 5, and 7 and $\theta = 0°$, 60°, and 120°. Here, for curved spherocylinders the orientation angle γ is defined as the angle that is formed by the line joining the centers of the two primary spheres at the ends of the particle and the horizontal axis of the system (for the particle sketched in Fig. 1c $\gamma = 0°$). When compared to packings of straight particles, particle curvature reduces the preference for horizontal particle alignment and increases instead the likelihood for vertical alignment, in particular for higher aspect ratios. For curved spherocylinders the particle orientation distribution is not symmetric around the vertical axis, although the horizontal orientation (0° or 180°) is always favored. Note, we can observe generally that curved particles have a higher probability for particle orientations in the yellow region (centered at 300° and 60°) than in the green region (centered at 120° and 240°). We speculate that this asymmetry is due to the sequential deposition process used here. Let us assume that particle **A** is located at the top of the pile (Fig. 8a), i.e. its concave side faces upwards ($\gamma = 180°$). If a depositing particle **B** approaches now the top of the pile with its concave side facing downwards (e.g. $\gamma = 45°$), the spherical-shaped "end" of particle **B** can get trapped into the "cavity" of particle **A** (Fig. 8b). Subsequently, Particle **B** rotates until it finds a stable local configuration, resulting in an orientation angle close to $\gamma = 0°$ (Fig. 8c). Such a configuration is more likely for particles with a high angle of curvature (i.e. $\theta = 180°$). Indeed, in particles with a high angle of curvature this asymmetry in the particle orientation distribution is more noticeable (Fig. 7). For other "depositioning angles", i.e. $90° - 270°$, particle **B** rotates until it has obtained an orientation angle close to 180°. For an intermediate angle of curvature i.e. $\theta = 60°$, we observe a higher tendency for a

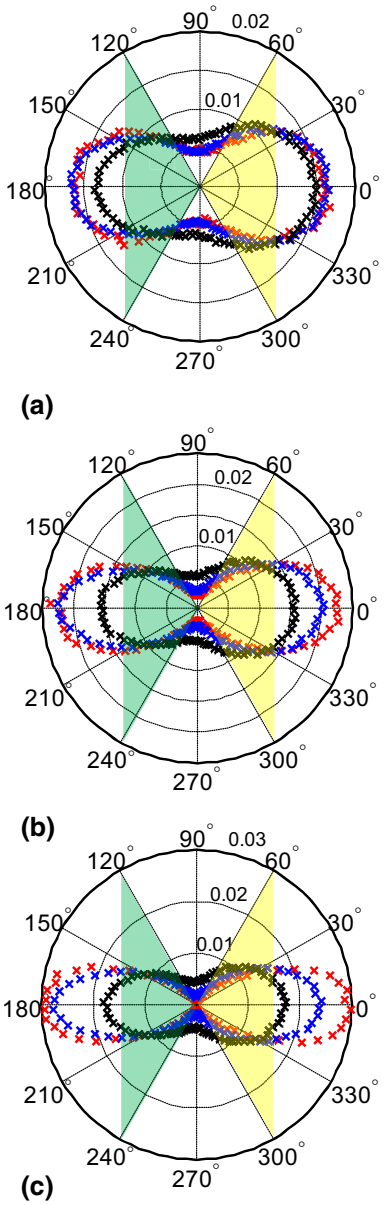

Fig. 7 Particle orientation distribution for curved spherocylinders: **a** $AR = 3$, **b** $AR = 5$, and **c** $AR = 7$. Packings of particles with the following angles of curvature were analyzed: $\theta = 0°$ (×), 60° (×), and 120° (×)

180° orientation than a 0° alignment for curved spherocylinders. This can be explained by a reduced interlocking effect. As the center of mass does not lie on the axis of the particle, under gravity a vertically standing particle has a high probability to rotate such that the convex side of the particle faces downwards. This would explain the preferred 180° orientation for such particles.

In Fig. 9 the RDFs for $AR = 3$, 5, and 7 and $\theta = 0°$, 60°, and 120° are plotted. Sketches exemplifying local packing configurations (corresponding to peaks in the RDFs) are included for visualization. Our numerical results indicate that

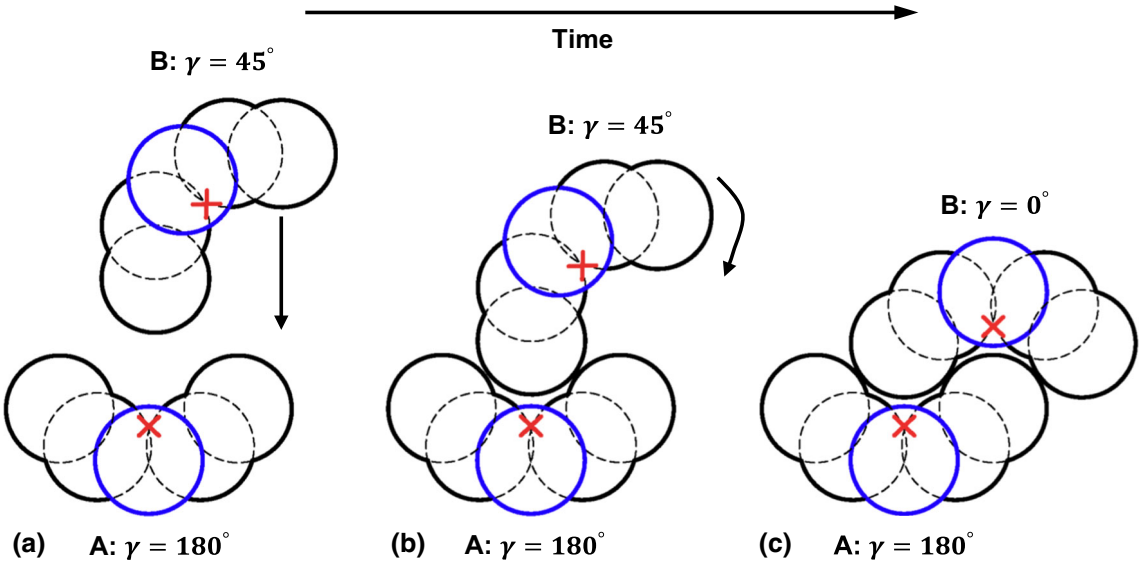

Fig. 8 Schematic sketches showing the interlocking of two particles for curved spherocylinders ($AR = 3, \theta = 120°$): **a** particle **B** ($\gamma = 45°$) approaches the previously deposited particle **A** ($\gamma = 180°$) located at the top of the pile; **b** the spherical-shaped "end" of particle **B** is trapped in the "cavity" of particle **A**; **c** particle **B** rotates until a stable configuration is obtained, i.e. $\gamma = 0°$. The central primary sphere of the individual spherocylinder is marked in blue, and the center of mass of the spherocylinder is marked with a '×' (colour figure online)

short range ordering is prevented by particle's curvature. This observation is consistent with the shape of the particle orientation distribution (Fig. 7), and confirms that curvature hinders the alignment of elongated spherocylinders in the horizontal direction. Consequently, large voids are generated between local clusters, reducing, in turn, significantly the solid fraction in the bed. For higher aspect ratios viz. $AR = 5$ and 7, voids form also around convex particle alignments, as shown in the insets of Fig. 9b, c. In particular, for particles with $AR = 7$ the peaks in the RDFs indicate that clusters comprising three aligned particles are commonly encountered. On the other hand, in packings composed of particles with $AR = 3$ and a large angle of curvature viz. $\theta = 120°$, the space on the concave side of the particles is readily occupied by the spherical cap of a neighbouring particle (see Fig. 9a, peaks in the RDF at $r/d_p = 1.2$ and 1.5). Therefore, dense packings are obtained in such beds. This observation is in line with the average solid fraction obtained in packings of spherocylinders with $AR = 3$ and large curvature angles (Fig. 6a).

Finally we evaluate stress transmission in packings of curved spherocylinders. Figure 10 plots $P_0 = (\sigma_v + \sigma_h)/2$ as a function of packing depth h (normalized by d_p). For $AR = 3$ (Fig. 10a) we observe increasing saturation stresses for increasing curvature angles. This can be attributed to particle interlocking and the preferential horizontal alignment of elongated particles. As shown in Fig. 9a, these packings comprise of densely packed clusters in which the space on the concave side of a particle is readily occupied by the spherical cap of a neighboring particle. Such packing arrangements favor a vertical stress transmission leading to a reduced stress saturation with packing depth. For spherocylinders with $AR = 5$, curvatures seem to have very little influence on stress transmission, although there seems to be some trend for decreasing saturation stresses with increasing curvature angles. This trend holds also for particles with the highest aspect ratio simulated, i.e. $AR = 7$. We attribute this effect to a broader particle orientation distribution for curved spherocylinders with $AR = 7$, i.e. these particles do not align horizontally as preferably as do their straight counterparts (Fig. 7c). Thus, a direct, vertical, stress transmission is less favorable.

4 Conclusions and outlook

Two-dimensional packings of spherocylinders with different aspect ratios, surface shapes and curvatures were modelled using non-spherical DEM. The effect of surface shape and curvature on packing morphology and stress transmission was assessed in detail. The following conclusions can be drawn from this work:

- In a packing of spherocylinders surface shape influences appreciably the particle orientation distribution. For example, straight, rough spherocylinders with $AR = 2$ exhibit a distinct preference for particle orientations $\gamma = 0°$, 30°, 90°, 150°, and 180°. These characteristic

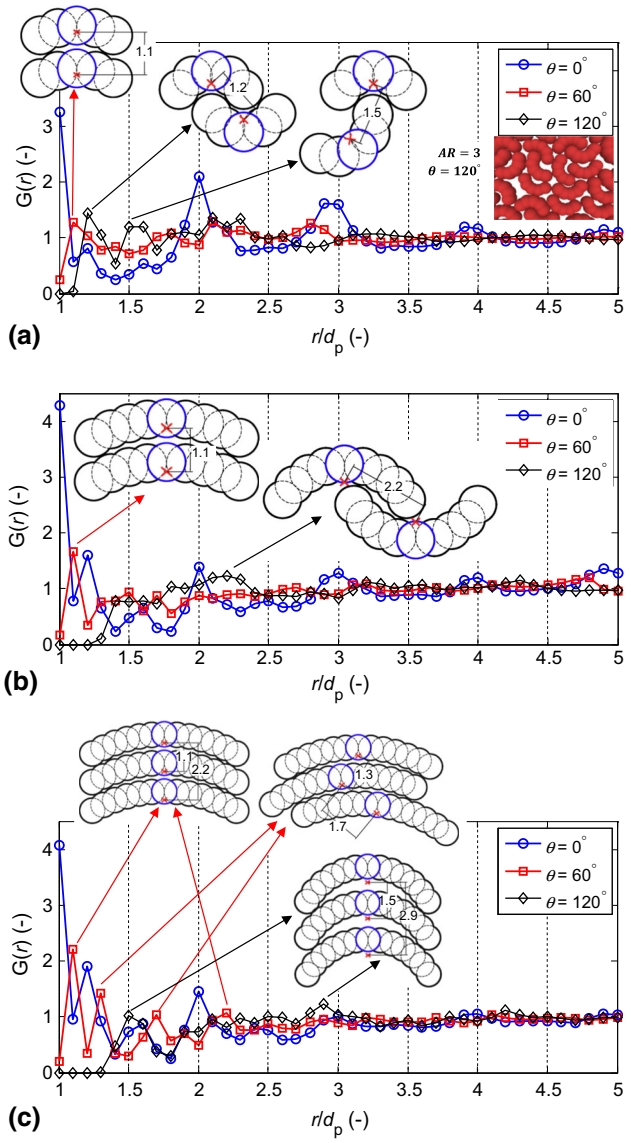

Fig. 9 Radial distribution function (RDF) for packings of curved spherocylinders: **a** $AR = 3$, **b** $AR = 5$, and **c** $AR = 7$ ('◯': $\theta = 0°$; '□': $\theta = 60°$; '◇': $\theta = 120°$). Specific packing configurations that correspond to peaks in the RDFs are sketched. The central primary sphere of the individual spherocylinder is marked in *blue*, and the center of mass of the spherocylinder is marked with a '×'. For $AR = 3$ and $\theta = 120°$ also a section of the packing simulated is shown. Packing configurations that correspond to peaks in the RDF at $r/d_p = 1.2$ and 1.5 can be observed in this inset (colour figure online)

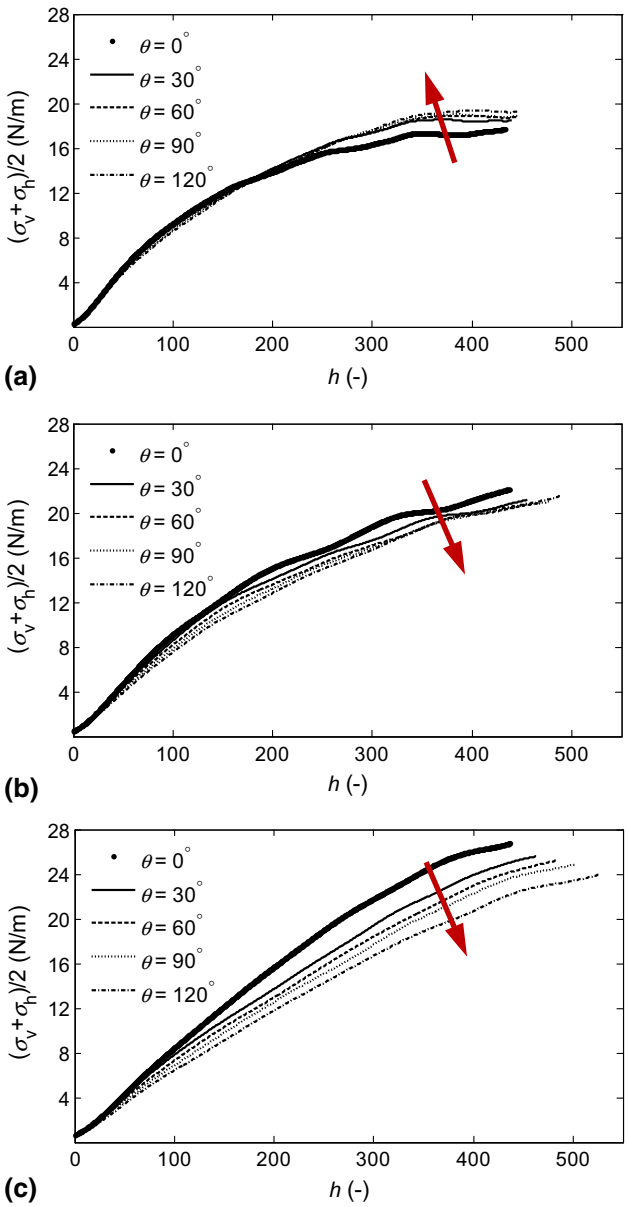

Fig. 10 $P_0 = (\sigma_v + \sigma_h)/2$ as a function of the dimensionless packing depth h (normalized by d_p) for packings of straight and curved spherocylinders: **a** $AR = 3$, **b** $AR = 5$, and **c** $AR = 7$

orientation angles indicate the presence of locally ordered structures. In contrast, packings of smooth particles gave a more continuous particle orientation distribution. A general finding was that elongated particles tend to align horizontally leading to a direct, vertical stress transmission. In addition, due to enhanced particle interlocking effects, coarse particles favor a direct vertical stress transmission when compared to smooth particles of identical aspect ratio. However, the influence of surface shape on packing morphology and stress transmission becomes almost negligible for highly elongated particles, i.e. particles with $AR = 5$ or 7.

- Particle curvature leads to a fairly continuous particle orientation distribution. This is in contrast to the preference for horizontal alignment commonly observed for straight, elongated particles. In addition, curvature enhances the probability for particles facing each other with their concave sides and convex particle alignment ("excluded volume" effect). Owing to the less likely horizontal alignment of elongated and curved particles ($AR = 5$ and 7), stress transmission is directed to a smaller extent into the

vertical direction. However, for $AR = 3$, an increasing curvature leads to an increasing saturation stresses. This is due to an increased tendency for particle interlocking.

To increase the practical relevance of this work further, its extension to 3D is required. In addition, the formation of a granular packing by discharging through an orifice or an inclined surface will be an interesting extension of this work. It is expected that also for such systems the surface shape and the curvature of the particles will influence appreciably the packing's morphology and stress transmission characteristics.

Acknowledgments The authors are grateful to the Swiss National Science Foundation (200021_132657/1) and the China Scholarship Council (Guang Lu) for partial financial support of this work. R.C. Hidalgo acknowledges the financial support from Ministerio de Economía y Competitividad (Spanish Government) through FIS2011-26675 and FIS2014-57325 Projects.

References

1. Torquato, S., Stillinger, F.H.: Jammed hard-particle packings: from Kepler to Bernal and beyond. Rev. Mod. Phys. **82**, 2633–2672 (2010)
2. Müller, C.R., Davidson, J.F., Dennis, J.S., Fennell, P.S., Gladden, L.F., Hayhurst, A.N., Mantle, M.D., Rees, A.C., Sederman, A.J.: Real-time measurement of bubbling phenomena in a three-dimensional gas-fluidized bed using ultrafast magnetic resonance imaging. Phys. Rev. Lett. **96**, 154504 (2006)
3. Cundall, P.A., Strack, O.D.L.: A discrete numerical model for granular assemblies. Géotechnique **29**, 47–65 (1979)
4. Zhu, H.P., Zhou, Z.Y., Yang, R.Y., Yu, A.B.: Discrete particle simulation of particulate systems: theoretical developments. Chem. Eng. Sci. **62**, 3378–3396 (2007)
5. Zhu, H.P., Zhou, Z.Y., Yang, R.Y., Yu, A.B.: Discrete particle simulation of particulate systems: a review of major applications and findings. Chem. Eng. Sci. **63**, 5728–5770 (2008)
6. Lu, G., Third, J.R., Müller, C.R.: Critical assessment of two approaches for evaluating contacts between super-quadric shaped particles in DEM simulations. Chem. Eng. Sci. **78**, 226–235 (2012)
7. Lu, G., Third, J.R., Müller, C.R.: Effect of particle shape on domino wave propagation: a perspective from 3D, anisotropic discrete element simulations. Granul. Matter **16**, 107–114 (2014)
8. Lu, G., Third, J.R., Müller, C.R.: Effect of wall rougheners on cross-sectional flow characteristics for non-spherical particles in a horizontal rotating cylinder. Particuology **12**, 44–53 (2014)
9. Börzsönyi, T., Stannarius, R.: Granular materials composed of shape-anisotropic grains. Soft Matter **9**, 7401–7418 (2013)
10. Lu, G., Third, J.R., Müller, C.R.: Discrete element models for non-spherical particle systems: from theoretical developments to applications. Chem. Eng. Sci. **127**, 425–465 (2015)
11. Baule, A., Makse, H.A.: Fundamental challenges in packing problems: from spherical to non-spherical particles. Soft Matter **10**, 4423–4429 (2014)
12. Langston, P.A., Al-Awamleh, M.A., Fraige, F.Y., Asmar, B.N.: Distinct element modelling of non-spherical frictionless particle flow. Chem. Eng. Sci. **59**, 425–435 (2004)
13. Wouterse, A., Luding, S., Philipse, A.P.: On contact numbers in random rod packings. Granul.Matter **11**, 169–177 (2009)
14. Kyrylyuk, A.V., van de Haar, M.A., Rossi, L., Wouterse, A., Philipse, A.P.: Isochoric ideality in jammed random packings of non-spherical granular matter. Soft Matter **7**, 1671–1674 (2011)
15. Zhao, J., Li, S.X., Zou, R.P., Yu, A.B.: Dense random packings of spherocylinders. Soft Matter **8**, 1003–1009 (2012)
16. Meng, L.Y., Li, S.X., Lu, P., Li, T., Jin, W.W.: Bending and elongation effects on the random packing of curved spherocylinders. Phys. Rev. E **86**, 061309 (2012)
17. Meng, L.Y., Lu, P., Li, S.X., Zhao, J., Li, T.: Shape and size effects on the packing density of binary spherocylinders. Powder Technol. **228**, 284–294 (2012)
18. Deng, X.L., Davé, R.N.: Dynamic simulation of particle packing influenced by size, aspect ratio and surface energy. Granul. Matter **15**, 401–415 (2013)
19. Nan, W.G., Wang, Y.S., Ge, Y., Wang, J.Z.: Effect of shape parameters of fiber on the packing structure. Powder Technol. **261**, 210–218 (2014)
20. Alonso-Marroquin, F.: Spheropolygons: a new method to simulate conservative and dissipative interactions between 2D complex-shaped rigid bodies. Europhys. Lett. **83**, 14001 (2008)
21. Hidalgo, R.C., Zuriguel, I., Maza, D., Pagonabarraga, I.: Role of particle shape on the stress propagation in granular packings. Phys. Rev. Lett. **103**, 118001 (2009)
22. Hidalgo, R.C., Zuriguel, I., Maza, D., Pagonabarraga, I.: Granular packings of elongated faceted particles deposited under gravity. J. Stat. Mech. Theory Exp. **6**, 06025 (2010)
23. Hidalgo, R.C., Kadau, D., Kanzaki, T., Herrmann, H.J.: Granular packings of cohesive elongated particles. Granul. Matter **14**, 191–196 (2012)
24. Azéma, E., Radjaï, F.: Stress-strain behavior and geometrical properties of packings of elongated particles. Phys. Rev. E **81**, 051304 (2010)
25. Azéma, E., Radjaï, F.: Force chains and contact network topology in sheared packings of elongated particles. Phys. Rev. E **85**, 031303 (2012)
26. Kanzaki, T., Acevedo, M., Zuriguel, I., Pagonabarraga, I., Maza, D., Hidalgo, R.C.: Stress distribution of faceted particles in a silo after its partial discharge. Eur. Phys. J. E **34**, 133 (2011)
27. https://upload.wikimedia.org/wikipedia/commons/a/aa/Fusilli_pasta.jpg
28. http://www.casabufala.it/wp-content/uploads/2014/11/bg_mezzani-tagliati-rigati1.jpg
29. http://dreamlandapparel.com/wp-content/uploads/2011/08/Macaroni-noodles.jpg
30. Goldhirsch, I.: Stress, stress asymmetry and couple stress: from discrete particles to continuous fields. Granul. Matter **12**, 239–252 (2010)
31. Acevedo, M., Zuriguel, I., Maza, D., Pagonabarraga, I., Alonso-Marroquin, F., Hidalgo, R.C.: Stress transmission in systems of faceted particles in a silo: the roles of filling rate and particle aspect ratio. Granul. Matter **16**, 411–420 (2014)
32. Weinhart, T., Thornton, A.R., Luding, S., Bokhove, O.: From discrete particles to continuum fields near a boundary. Granul. Matter **14**, 289–294 (2012)
33. Zou, R.P., Yu, A.B.: Evaluation of the packing characteristics of mono-sized non-spherical particles. Powder Technol. **88**, 71–79 (1996)
34. Janssen, H.A.: Versuche über Getreidedruck in Silozellen, Verein Deutscher Ingenieure. Zeitschrift (Dusseldorf) **39**, 1045–1049 (1895)